PROGRESS IN COLOR, COLORANTS AND COATINGS

available online @ www.pccc.icrc.ac.ir

Progress in Color Colorants Coating 19 (2026), 485-506

Ministry of Science, Research and Technology
Institute for Color Science & Technology

Polyurethane-based Nanocomposite Film as Barrier Coating: Effect of Weight Content of TiO_2 Nanoparticles on the Surface Wettability, Moisture Permeability, Mechanical Durability, and Thermal Stability

N. Karimi, A. Bahramian*
Chemical Engineering Department, Hamedan University of Technology, P.O. Box: 65155, Hamedan, Iran.

ARTICLE INFO

Article history:
Received: 12 Oct 2025
Final Revised: 04 Dec 2025
Accepted: 06 Dec 2025
Available online: 04 May 2026

Keywords:
Polyurethane@TiO_2
Nanocomposite
Coating material
Surface wettability
Moisture permeability
Thermomechanical stability

ABSTRACT

The surface wettability, moisture permeability, mechanical durability, and thermal stability of polyurethane (PU) and PU@TiO_2 nanocomposite films at different weight contents of TiO_2 nanoparticles (NPs) were studied experimentally. An increase in the NPs wt. % led to an increase in the hydrophobic property, thermal stability and mechanical durability of the films. The water contact angle (WCA) increased from 94.7° to 98.9° with the films' surface roughness due to NP agglomeration. The curing temperature (T_c) influenced the films wettability at $T_c \leq 140$ °C, while film surface segregation was observed at $T_c > 160$ °C. The WCA of pure PU increased from 93.4° to 107.1° with an increase in T_c from 60 to 200 °C, respectively. Moisture permeability improved with the incorporation of 5 wt. % NPs. Due to the more porous structure of the 7 wt.% sample, its water absorption rate was slightly higher than that of the 5 wt.% sample. The glass transition temperature and melting temperature of the 7 wt.% sample were 88.2 and 185.5 °C, respectively, while the enthalpy of fusion was determined to be 22.82 J/g. The tensile strength and elongation at the break of the films slightly decreased with an increase in the NPs wt. %. The kinetic model of water absorption indicated that the effective diffusion coefficient (D_{eff}) is highly influenced by the porous structure of the film. D_{eff} decreased from 2.4×10^{-8} to 1.4×10^{-10} $cm^2.s^{-1}$ as the NP weight content increased from 3 to 7 wt.%, while the permeability coefficient (P_{eff}) exhibited an increase from 3.2×10^{-11} to 8.0×10^{-11} $mg.cm(Pa.s)^{-1}$. Additionally, relative humidity showed a greater effect on D_{eff} than NP weight content, while the opposite was observed for P_{eff}. Prog Color Colorants Coat. 19 (2026), 485-506© Institute for Color Science and Technology.

1. Introduction

Polyurethane (PU), found by the Otto Bayer reaction of polyol (a soft component) and isocyanate (a hard component) [1], is a type of thermoplastic polymer with desirable characteristics such as low density, high durability, and flexibility [2, 3]. However, its disadvantages include low thermal stability and mechanical strength. The surface wettability, moisture permeability, and thermal stability of PU-based nanocomposite films are important in practical applications such as packaging, medical devices, foams, barrier coatings, footwear, rigid insulators, and industrial machinery [4-7]. Furthermore, due to its acceptable flexibility, PU is an ideal coating material

*Corresponding author: * bahramian@hut.ac.ir
https://doi.org/10.30509/pccc.2025.167696.1460

for protecting the surfaces of complicated fittings used in fluid transport systems [8].

The modification of polymeric coating properties through the incorporation of nanoparticles (NPs) as nanocomposite films can enhance desirable characteristics while mitigating inherent weaknesses [9-11]. The chemical and physical properties of NPs significantly influence the mechanical and thermal performance of the resulting nanocomposite [10]. Achieving a reduction in moisture permeability, alongside an improvement in the hydrophobicity and thermal stability of nanocomposite films, remains a challenging objective due to the associated decline in the mechanical properties of pure PU [12]. A literature survey shows NPs such as carbon nanotubes [13], SiO_2 [14], ZnO [15], and TiO_2 [16] have been physically blended and chemically modified in PU hybrid nanocomposites.

During the fabrication of PU nanocomposite films, NPs predominantly tend to segregate from the polymer matrix throughout the blending process, resulting in a non-homogeneous phase structure [15, 16]. Owing to the van der Waals (vdW) force, NPs tend to agglomerate, which can adversely impact the properties of the nanocomposite film [18]. Therefore, achieving a uniform dispersion of NPs within the polymer matrix constitutes a primary challenge in the production of nanocomposite films [12]. Bahramian [17] showed that homogeneous incorporation of TiO_2 NPs into the polymer phase structure led to enhancements in thermal resistance, glass transition temperature (T_g), and mechanical properties of PET@TiO_2 nanocomposite films.

The weight content (%) of NPs significantly influences the properties of nanocomposite films [16-18]. Pegoretti *et al*. [18] showed a notable enhancement in Young's modulus; tensile strength and wear resistance were achieved by incorporating a 1 wt. % by-weight content of ZnO NPs into the PU matrix, resulting in a better morphological structure than the sample containing 5 wt. %. Burgaz *et al*. [19] reported that the sample containing a hybrid of 0.4 wt. % multiwall carbon nanotubes (MWCNT) and 0.1 wt. % nanosilica has a higher glass transition temperature (T_g) value, a superior storage modulus at T_g, and better thermal stability than the sample containing only 0.5 wt. % MWCNT. Krol *et al*. [16] proposed that TiO_2 NPs act as a plasticizer agent within the soft phase of PU, increasing the mobility of polymer chains, which resulted in a decrease in the T_g of PU@TiO_2 films from -28 to -40 °C. Variations in the weight percentage (wt. %) of TiO_2 NPs induced changes in the physical interactions between the soft and hard phases of the PU matrix, thereby reducing the degree of phase separation [16]. Consequently, given the high surface sensitivity of nanocomposite films to NP incorporation, it is imperative to thoroughly investigate all factors influencing the properties of PU@TiO_2 nanocomposite films.

The moisture permeability of barrier coatings is a critical parameter in determining the stability of PU nanocomposite films during prolonged exposure to humid environments. Several parameters, including the concentration gradient of water molecules, pore size, tortuosity, free volume, density, film thickness, surface energy, and contact angle, influence the moisture permeability of the film [4, 14, 20-22]. The higher the density of the film, the smaller the average pore size, and the larger the film thickness, thus providing better water resistance. A lower contact angle results in higher moisture permeability and lower hydrophobic properties of the film surface [23]. The moisture absorption (%) of nanocomposite films significantly affects the mechanical, physical, and thermal properties of nanocomposite films [19, 24].

TiO_2 NPs have shown a broad range of practical applications as filler or reinforcement agents due to their nano-scale size, low toxicity, and antibacterial activity [24]. In many cases, improving one property leads to a decrease in other properties [24-25]. The addition of TiO_2 NPs led to significant improvements in the surface hydrophobicity, mechanical strength, and antimicrobial efficacy of polymeric films, which have given them increasing interest in various industries, including automotive, marine, and medical practical applications [25]. The compatibility of TiO_2 NPs enables an improved heat resistance structure of the polymer matrix, in which the high dielectric constant property of TiO_2 plays an important role in the later degradation of the PU@TiO_2 nanocomposite [15]. The moisture permeability of pure PU decreases with the incorporation of TiO_2 NPs, while the thermal stability of PU@TiO_2 nanocomposite significantly improves as the TiO_2 NP content increases from 5 to 10 wt. % compared to the virgin polymer; however, it declines with further additions of nanoparticles (NPs). Modifications in the surface structure of the resulting nanocomposite also impact the surface wettability of

the films. The maximization of the properties in nanocomposite is due to the drastic increase in the contact surface between the matrix of polymer and filler [26]. The degree of surface wetting is directly related to both moisture permeability and thermal stability of the nanocomposite film [24]. There is no comprehensive study that considers all the thermal stability, moisture permeability, surface wettability, and thermomechanical properties of the reinforced PU@TiO_2 coating. Therefore, determining the optimal TiO_2 wt. % within the PU@TiO_2 nanocomposite films is essential for developing an effective coating that balances mass and heat transfer phenomena.

Within the experimental framework, kinetic models related to water sorption and surface wettability have been developed based on Fick's diffusion law to determine the diffusion coefficient of water molecules within the nanocomposite film, particularly concerning the significance of water mass change (%) at extended exposure times [26-28]. Water sorption isotherms, derived from theoretical models such as the Brunauer-Emmett-Teller (BET) theory, were utilized to elucidate the sorption mechanisms and calculate the corresponding diffusion coefficients in complex hybrid systems [28]. The findings from both kinetic and equilibrium sorption studies enhance the characterization of a sorption mechanism involving the phenomenon of water clustering [29].

In this study, the effect of the weight content (%) of TiO_2 NPs (0, 3, 5, and 7 wt. %) on the surface wettability, moisture permeability, and thermal stability of the prepared PU@TiO_2 nanocomposite films was studied to evaluate their applicability as barrier coatings. The results are presented in experimental and theoretical sections: In the experimental section, (1) the surface wettability, moisture permeability, and thermal stability of pure PU and PU@TiO_2 nanocomposite films were assessed through contact angle measurements, moisture absorption tests, and TGA-DTG analysis, respectively; (2) The water absorption was determined experimentally by immersing of the samples in water for a period of 30 days to determine the mass variations of samples during experiments. (3) A two-way analysis of variance (ANOVA) was conducted to evaluate the reliability of experimental data. In the theoretical part, (1) the relationship between moisture absorption with time, which describes the change in the concentration gradient of moisture content in the film over time, was determined based on Fick's second law, (2) the kinetic model of water absorption, which is calculated based on the film thickness, is analyzed using a quantitative theoretical model to determine the effective diffusivity coefficient (D_{eff}) and effective permeability coefficient (P_{eff}) of water vapor in the samples at relative humidity (*RH*) values of 50, 60, 70, 80, and 90 % at 25 °C.

2. Experimental

2.1. Materials

Granulated PU elastomer (Desmopan 2590A) with a density of 1102.5 kg/m³ was purchased from Bayer Material Science. Tetrahydrofuran (THF), sodium hydroxide (NaOH, ≥97 %), nitric acid (HNO_3, 63 %), and ethanol (EtOH, 99.9 %) were supplied by Merck (Darmstadt, Germany). Commercial hydrophobic titanium dioxide (AEROXIDE, TiO_2, 99.9 %) NPs, with a mean size of 21 nm (size range of 10-80 nm), a true density of 4.506 g/cm³, and a specific surface area of 50 m²/g, were provided by Evonik Industries Co. (Essen, Germany).

2.2. Preparation of substrates

First, the steel plates (SS304) with a thickness of 0.5 mm were cut into uniform sizes (5×5 cm^2). Then, the substrates underwent a three-step cleaning process. Initially, the steel plates were subjected to ultrasonic cleaning in EtOH for 15 min to eliminate any contaminants. Next, the substrates were immersed in 1 M NaOH for 20 min to remove organic pollutants and achieve a clean surface. Subsequently, the substrates were placed in a thermal oven at 200 °C for 15 min to ensure thorough cleaning. Finally, the substrates were allowed to cool to room temperature and were prepared for film application.

2.3. Preparation of nanocomposite films

A specific quantity of PU granules (5.74 g) was dissolved in 115 mL THF, as a water-miscible solvent, to create 5 wt. % PU solutions (designated as solution A). An electrostatic spraying device (NEW KCL-CU801 model, Shenzhen Hongheida Instrument Co., China) was employed to produce uniform films. A series of comparable samples were prepared with an isocyanate index (NCO/OH) of 1.3:1.0, utilizing THF as a diluent.

The PU solution (Solution A) was sprayed onto the substrates with a 40-psi compressed airflow through a

spray gun at a spraying distance of 10 cm to achieve a pure PU film. The spraying time varied between 70-90 seconds, depending on the required thickness. The pure sample was allowed to dry under ambient conditions. To create the PU@TiO_2 nanocomposite film, a TiO_2 solution (Solution B) was prepared by dissolving TiO_2 NPs (3.0, 5.0, and 7.0 wt. %) in a mixture of deionized water and ethanol with a ratio of 3:1, with vigorous stirring at 45 °C for 2 h. At the same time, HNO_3 0.3 M was added dropwise to solution B. Finally, the final solution was heated and refluxed at 80 °C for 24 h until a stable and homogeneous solution was obtained, indicating that the TiO_2 NPs were well dispersed in solution B. Solution A was thoroughly mixed with solution B completely for 30 min to form the final mixture. A series of PU@TiO_2 nanocomposite films (PU2-4) were prepared using the spraying method. The weight content of TiO_2 NPs was selected based on previous results, which indicated that incorporating values greater than 7.0 wt.% led to NP agglomeration and inhomogeneity in the nanocomposite film [7]. Finally, the samples were cured at various curing temperatures (T_c), ranging from 60 to 200 °C with a temperature interval of 20 °C.

For further reference, the samples of pure PU, PU@TiO_2 (3.0 wt. %), PU@TiO_2 (5.0 wt. %), and PU@TiO_2 (7.0 wt. %) are designated as PU1, PU2, PU3, and PU4, respectively. The PU films (PU1-PU4) were applied to the substrate in a completely homogeneous manner, maintaining a constant thickness of 1.5 mm. The distance between the film surface and the nozzle was set to 100 mm (±10 mm). The gelling time of the coating at 25 °C was approximately 2.5 min, while the surface curing time of the film was 30 min. The final drying process for the films typically took 6 days. After this period, the residual moisture content on the film surface evaporated, and the samples were stored in a dry environment for analysis.

2.4. Sample analysis and characterization

2.4.1. Surface characteristics and thickness of films

A transmission electron microscope (TEM, Zeiss EM900) was employed to analyze the surface structure and dispersion of NPs in the polymer matrix of the films. The mapping analysis, which represents the distribution of TiO_2 NPs within the polymer matrix was examined using scanning electron microscopy coupled with energy-dispersive X-ray spectroscopy (SEM/EDS, Hitachi SU 5000). The topographical structure of the nanocomposite films (PU1-4) was determined by AFM (model: ARA Research-BRISK 2019). The surface topography of the films and their surface roughness were determined by AFM analysis. Additionally, the thickness of the films was measured by a laser ellipsometer (SE 800 PV model, SENTEC).

2.4.2. Contact angle and penetration time tests

The surface wettability and degree of hydrophobicity of the films were analyzed using a video-based water contact angle (WCA) measurement system (OCA 15, Dataphysics Instruments GmbH, Germany). The WCA of the samples was measured before and after their placement in a thermal oven under vacuum conditions. Water droplet penetration time experiments were conducted by dropping 10 µL of water droplets onto the surface of samples to assess their absorption capacity for moisture molecules. The WCA values were measured using the method proposed by Zisman [30] using an optical goniometer with a digital camera positioned along the axial extension of its lens. Measurements were taken on both dry and wet surfaces after 24 h to determine the optimal conditions for achieving a hydrophobic surface.

2.4.3. Moisture permeability test

The absorption of water by the samples (PU1-4) was measured using a weight method (ASTM D5229, Moisture Absorption of Matrix Composites) at 23 °C under equilibrium conditions. Before the moisture permeability test, the samples were dried in air for 2 hours at a temperature of 23 °C and a relative humidity (*RH*) of 38 %, followed by drying in an oven for 24 hours at a temperature of 40 °C. The thickness of the films was measured by a laser ellipsometer according to procedure described in section 2.4.1. The variations in the moisture content of the samples over time were determined using a digital scale. The mass change of water absorbed by the sample, M, was calculated using the following formula (Eq. 1).

$$M = \frac{(W_i - W_0)}{W_0} \times 100 \quad (1)$$

where w_i and w_0 are the masses of the sample after and before immersion in water, respectively. The measurements were taken as the arithmetic mean of three values obtained with the same duration of immersion in water.

The moisture permeability test was conducted by immersing the samples in water, and the amount of water absorbed by the samples was measured over a period of one month. The moisture content absorbed per unit surface area per unit time was calculated over 30 days, expressed in g/m²/day. The samples were conditioned in a climatic chamber maintained at 25 °C and 50 % *RH* for a minimum of 2 days. In this condition, the samples reached equilibrium conditions. Subsequently, the samples were dried in a screw-cap filled with silica gel. The uptake of water vapor by the silica gel resulted in an increase in the weight of the samples. Each measurement was recorded at 50, 60, 70, 80, and 90 % *RHs* at 25 °C. The experiments were repeated twice to minimize measurement errors. The water vapor transmission rate (WVTR) is calculated using the following equation (Eq. 2) [31].

$$WVTR = \frac{(W_i - W_0)}{t\,A} \quad (2)$$

where t is the period of time between two weight measurements in h, and A is the measuring area in cm^2. P_{eff} is obtained from the following formula (Eq. 3) [27].

$$P_{eff} = \frac{WVTR}{P\,(R_1 - R_2)} \times l \quad (3)$$

where l is the film thickness, P is the vapor pressure of water at 25 °C, and R_1 and R_2 are moisture gradients.

2.4.4. Thermal stability analysis

The thermal stability of the samples was analyzed by a TGA/DTG analyzer (Perkin-Elmer Instrument, Pyris 1). TGA/DTG experiments were conducted in a high-purity nitrogen atmosphere with a heating rate of 10 °C/min over a temperature range of 25 to 600 °C. The weight of the samples varied from 5.82 to 6.01 g, depending on the weight content of TiO_2 NPs. Dynamic mechanical thermal analysis (DMTA, TA Instruments, Model Q600) was used to study the thermomechanical tests. Stress-strain analysis was carried out on the films with a mean thickness of 1.5 mm at 25 °C. The deformation test was performed at a frequency of 1 Hz and a strain of 0.1 %. To obtain char residue (%), the weight of decomposed films cured at 600 °C was determined through the following reactions (Eqs. 4 and 5).

$$Nanocomposite\ film_{(s)} \rightarrow Volatile_{(g)} + Residue_{(s)} \quad (4)$$

$$Residue_{(s)} + O_2 \rightarrow Volatile_{(g)} + Char_{(s)} \quad (5)$$

2.4.5. Gel content (%) and solubility (%)

Gel content (%) is a key parameter indicating the degree of chemical crosslinking of a polymer compound. In this study, the gel content (%) was determined based on boiling of films in a sufficient amount of organic solvent (THF) for 12 h. After extraction, the THF was removed from the samples by soaking then in water, and then the samples were dried in a vacuum oven at 70 °C to obtain a film with a constant weight. The gel content (%) was calculated gravimetrically using the following equation (Eq. 6).

$$Gel\ content\ (\%) = (W_1 / W_2) \times 100 \quad (6)$$

where W_1 and W_2 were the dry weight of samples after extraction and the initial dry weight of samples, respectively. The solubility (%) of samples was determined as 100 - gel content (%).

3. Theoretical model

3.1. Assumptions and boundary conditions (BCs)

The primary assumptions and BCs are as follows:

(1) At t = 0, the concentration of water molecules within the sample is assumed to be zero.
(2) The upstream surface equilibrium is achieved instantaneously.
(3) The downstream surface desorption is instantaneous.
(4) The effects of the film's edge are neglected due to non-homogeneities in the results.
(5) The adsorption of water molecules on the film surface occurs rapidly, while diffusion within the polymer structure is the time-limiting step for the film's absorption rate.
(6) The polymer matrix does not react with water molecules.
(7) The film structure is isotropic at a macroscopic scale.

3.2. kinetic of water absorption

The relationship between moisture absorption (%) versus time (Eq. 7) was theoretically determined based on Fick's second law, which describes the change in the concentration gradient of moisture content in the film over time [27, 28].

$$\frac{\partial C}{\partial t} = \frac{\partial}{\partial x}\left(D\frac{\partial C}{\partial x}\right) \quad (7)$$

where *C* is the penetration concentration of water molecules, *t* denotes time, *x* indicates the vertical direction within the samples, and D is the diffusion coefficient of water molecules in the sample. The kinetic model of water sorption on the film surface is calculated based on the film thickness, *h*, according to the following equation (Eq. 8) [32].

$$\frac{M_t}{M_\infty} = \left(1 - \frac{8}{\pi^2}\sum_{n=0}^{\infty}\left[\frac{1}{(2n+1)^2}\exp\left(\frac{-D_{eff}\,\pi^2(2n+1)^2 t}{h^2}\right)\right]\right) \quad (8)$$

Where M_t is the water sorption at time *t*, M_∞ is the water sorption at the equilibrium state, and M_t/M_∞ is the relative mass fraction of water molecules within the film.

The early steps of the diffusion-controlled mechanism can be predicted by a simplified model for the determination of D_{eff} in the $M_t/M_\infty < 0.5$ (Eq. 9) [33].

$$\frac{M_t}{M_\infty} = \frac{4}{h}\cdot\sqrt{\frac{D_{eff}\,t}{\pi}} \quad (9)$$

for $M_t/M_\infty \geq 0.5$, D_{eff} can be obtained as follows (Eq. 10).

$$\ln\left(1 - \frac{M_t}{M_\infty}\right) = \ln\left(\frac{8}{\pi^2}\right) - \frac{\pi^2 D_{eff} t}{h^2} \quad (10)$$

D_{eff} can be graphically obtained from the measured absorption curves in the literature [27] by considering a simplification in equations 9 and 10, which are defined for short and long times, respectively. Dolmaire *et al*. [28] reported that the estimated error from the approximation applied in equation 10 as compared to equation 9 is about 0.1 %. In this study, equation 8 was utilized to determine D_{eff} in water absorption experiments. D_{eff} represents the diffusion constant of water molecules in the PU film. The fitting of equations 9 and 10 to the measured water mass change curves was performed using OriginPro software.

4. Results and Discussion

4.1. Experimental results

4.1.1. Morphological study

Figure 1 shows the TEM images of the surfaces of PU1, PU2, PU3, and PU4 samples cured at 80 °C for 30 min. The TEM images reveal that the films possess smooth and homogeneous surfaces, indicating effective mixing of PU granules in the THF solvent to form a uniform structure of PU nanocomposite films (left images). It is evident that the surfaces of the PU films are frequently filled by TiO_2 NPs. The bright spots in the images signify localized agglomeration of NPs within the polymer structure, which led to a decrease in the surface homogeneity of the samples. The number of bright spots increases with a higher weight fraction of NPs. Consequently, the surface homogeneity of the PU1 sample is better than that of PU4, attributed to the increased likelihood of local agglomeration at a higher weight percentage of TiO_2 NPs. Furthermore, the presence of surface inhomogeneities arises from tiny pores in the PU samples, which led to create crystalline regions and cross-linking of polymer, through joining of TiO_2 NPs to PU matrix structure.

Figure 2 shows the SEM analysis of the PU1, PU2, PU3, and PU4 films, and (e) EDS spectra of PU4 film, which were cured at 80°C for 30 min. The SEM results reveal differences among the samples in terms of percentage composition and distribution of the elements (see right images). The results confirmed that an increase in the weight percentage of TiO_2 NPs from 0 to 7.0 wt. % led to an increase in NP agglomeration. The peaks of the EDS spectra of the 7.0 wt. % sample showed three distinct peaks at 0.27, 0.41, and 0.68 keV, which represent the C, N, and O atoms, respectively (Figure 2e). The high absorbance peaks at 5.12 and 5.56 keV represent the Ti atoms of TiO_2 at the surface of the PU4 sample (Figure 2e). The EDS results showed that the atomic ratio between Ti and O was 61.4/38.6.

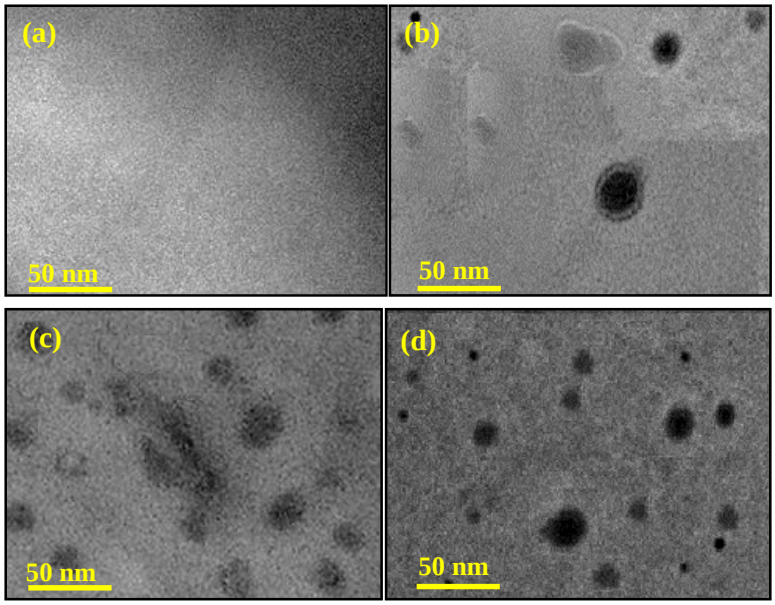

Figure 1: TEM images of (a) PU1, (b) PU2, (c) PU3, and (d) PU4 samples cured at 80 °C for 30 min.

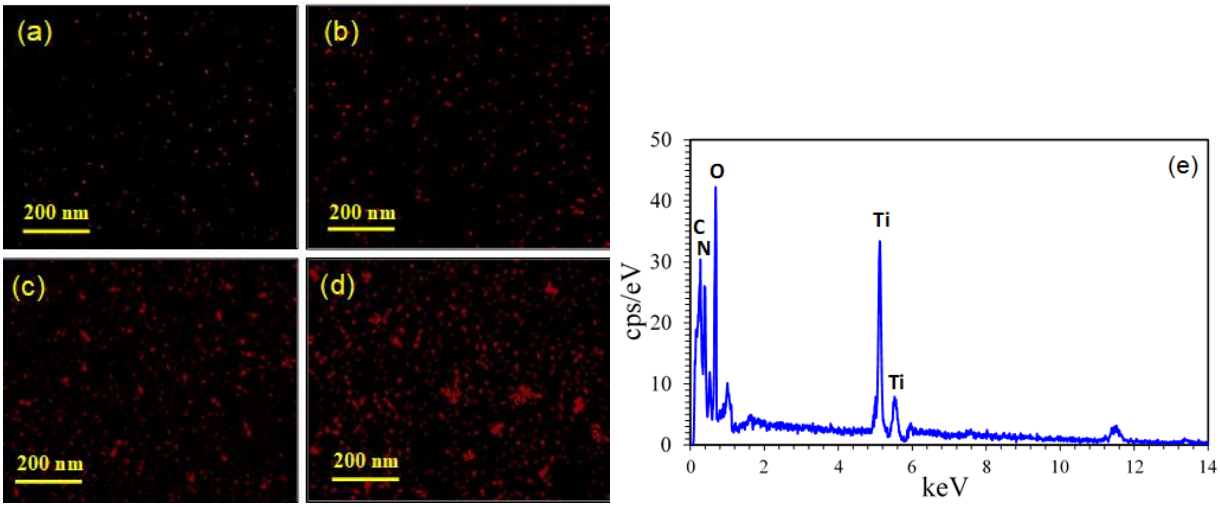

Figure 2: SEM analysis of (a) PU1, (b) PU2, (c) PU3, and (d) PU4 films, and (e) EDS spectra of PU4 film cured at 80 °C for 30 min.

Figure 3 presents three-dimensional AFM images of (a) PU1, (b) PU2, (c) PU3, and (d) PU4 films with a mean thickness of 1.5 mm when cured at 80 °C for 30 min. The images were acquired using the Inspects NanoSpace BRISK device and processed with AFM2018 software. The AFM analysis was conducted to identify the surface homogeneity and characterization of the prepared films. The AFM images reveal that the topographical structure of the samples is significantly influenced by the weight content of TiO_2 NPs. An increase in the weight content of NPs led to a decrease in the surface uniformity of the samples. The sharp peaks in the images indicate the presence of individual NPs, whereas the broad peaks signify the agglomeration of NPs. Furthermore, the NPs agglomeration decreases the effectiveness of NPs in the polymer matrix, which ultimately results in the poor properties of PU4 sample [34]. The pure sample (PU1) shows the smoothest surface, associated with the most homogeneous structure, while the mass fraction of 7.0 wt. % TiO_2 represents the roughest surface. The low number of sharp peaks in the nanocomposite samples suggests that the additive is well mixed into the polymer matrix. The presence of NPs has led to a form of PU@TiO_2 structure, which weakens the original PU bonds and contributes to the breakage of PU network chains.

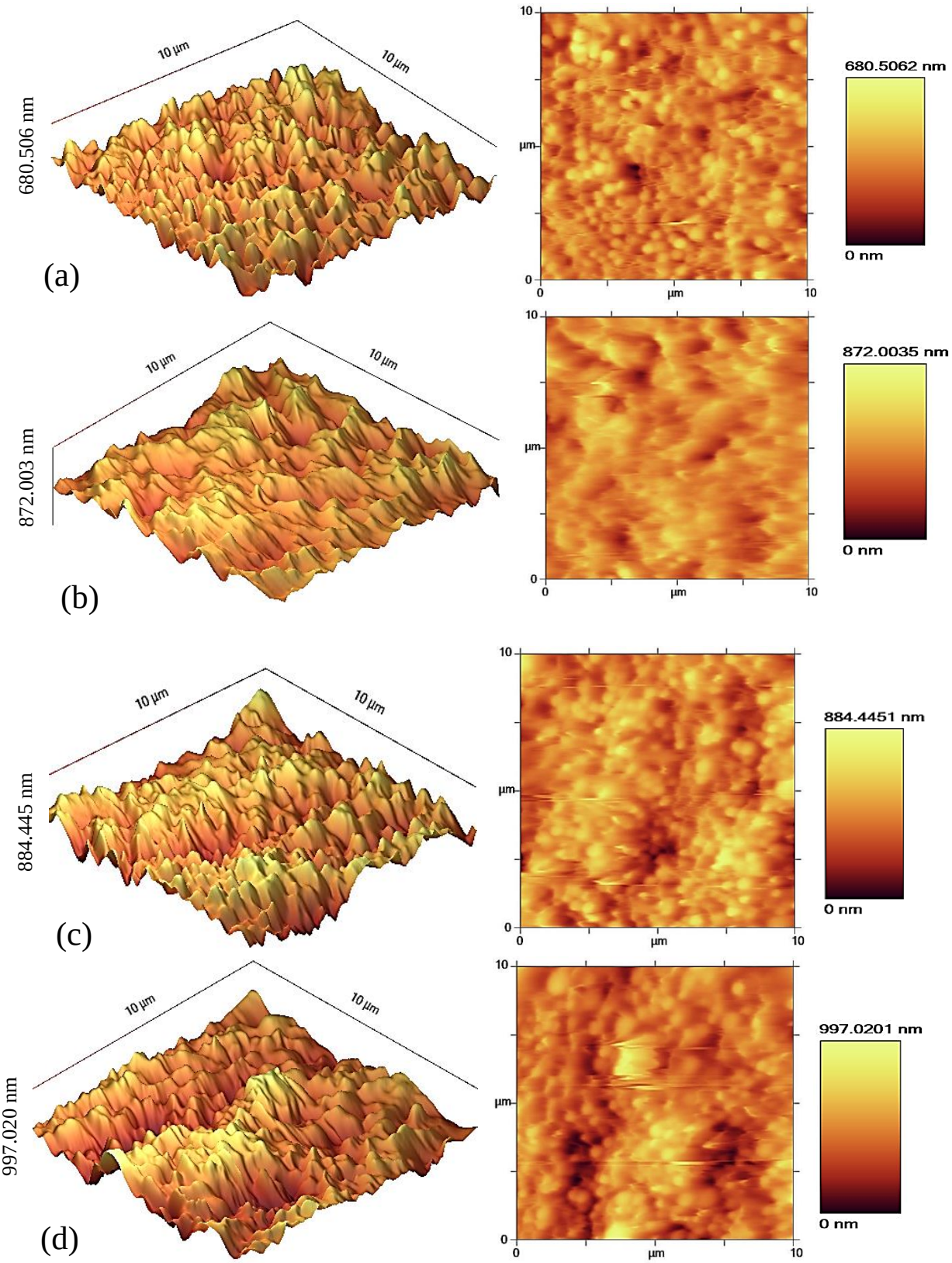

Figure 3: AFM images of (a) PU1, (b) PU2, (c) PU3, and (d) PU4 films cured at 80°C for 30 minutes [left and right figures represent the three-dimensional and two-dimensional AFM images, respectively].

Table 1 shows the results of the surface roughness parameters for PU1-4 samples cured at 80°C for 30 min. The uncertainty of the mean experimental data is shown in the table. The surface roughness of the films increases with a higher weight percentage of TiO_2 NPs. The high root-mean-square roughness (R_q) and average surface roughness (R_a) of the PU4 sample can be attributed to the tendency of TiO_2 NPs to form agglomerated structures on the surface of the nanocomposite film, as confirmed by AFM analysis (Figure 3d). The RMS of the PU4 sample is twice that of the PU1 sample. However, the PU4 sample shows a relatively low R_a value (~111 nm), indicating that the NPs induced only minor nano-structural changes in the sample's topography. Additionally, the difference between the valley roughness (R_v) and peak roughness (R_p) values is linked to the agglomeration of NPs, which contributed to the rise in the surface roughness parameters of the samples. The high R_q and R_a values of PU4 sample could be justified by the presence of large NP agglomerates on the film surface, which was confirmed by AFM images (Figure 3).

4.1.2. Surface wettability study

To determine the wettability of the samples, the WCA analysis was conducted on the surface of the PU nanocomposite films. Figure 4 shows microphotograph images of water droplets on the surface of (a) PU1, (b) PU2, (c) PU3, and (d) PU4 samples cured at 80 °C for 30 min. Figure S1 presents additional microphotographs of the water droplet profiles on the surface of the PU1 and PU4 samples, indicating the hydrophobic properties of the samples. Complete moisture permeability occurs at a contact angle of zero, while a film surface is considered water-resistant when the WCA value exceeds 90° [35]. The contact angle of the water droplet on the surface of the PU1 sample is 94.7°, indicating its relatively hydrophobic nature.

An increase in the TiO_2 NPs wt. % resulted in a higher contact angle for the samples, thereby enhancing the hydrophobicity of the films. A reduction in the hydrophobicity of the PU4 sample, caused by an increase in the weight content of TiO_2 NPs, can be attributed to two reasons: (1) The presence of TiO_2 NPs increased the surface energy of the PU nanocomposite film, which subsequently led to a higher WCA value and a decrease in the sliding angle. TiO_2 NPs, on a polar surface due to the presence of -OH groups, interact more strongly through hydrogen bonds with polar urethane hard segments [35]. (2) TiO_2 NPs can adhere to the PU matrix, creating rough and hydrophobic characteristics, with a contact angle of 98.9°. Wang *et al.* [36] reported that the hydrophobic properties of surfaces improve with increased roughness, leading to a higher contact angle as roughness decreases. The enhanced hydrophobicity of the nanocomposite film, resulting from the presence of modified TiO_2 NPs, led to an increase in platelet adhesion and a delayed degradation rate in wet environments [36].

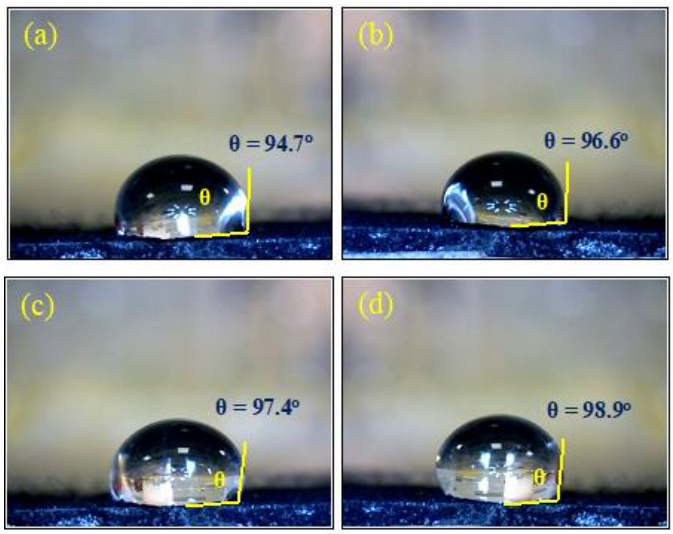

Figure 4: The microphotograph images of water drop on the surface of (a) PU1, (b) PU2, (c) PU3, and (d) PU4 samples cured at 80 °C for 30 min.

Table 1: Surface roughness results of PU1-4 samples cured at 80°C.

Roughness parameters	PU1	PU2	PU3	PU4
Root-mean-squared roughness (R_q, nm)	69.224±2.230	93.813±2.630	104.031±4.585	142.429±6.857
Average roughness (R_a, nm)	52.090±3.101	73.236±3.756	78.654±3.957	110.957±4.536
Valley roughness value (R_v, nm)	-355.866±8.785	-446.084±9.857	-453.475±10.859	-572.037±11.674
Peak roughness value (R_p, nm)	324.639±9.382	438.361±10.193	430.970±12.690	424.983±13.849

Figure 5 shows the results of WCA obtained from the PU1-4 samples at various T_c ranging from 60 to 200°C. The impact of thermal heating on the WCA values of the samples was analyzed during a curing process conducted in a thermal oven under vacuum conditions. Error bars indicate the standard deviation corresponding to at least three experimental data points. The WCA value of pure PU increased from 93.4° to 107.1° with an increase in T_c from 60 to 200 °C, respectively, indicating that an increase in T_c leads to an increase in the hydrophobicity of the PU nanocomposite film. This phenomenon can be attributed to the fact that at lower T_c the fluid interacted more with the film surface, resulting in a decrease in the WCA value. Notably, the values of WCA do not change significantly in T_c values between 180 and 200 °C. This observation is attributed to the reduced mobility of oligomer and polymer chains within the film decreases due to the high evaporation rate of the solvent, leading to the interlocking of the polymer chains in the film [36].

Error analysis results showed that the uncertainty of the experimental data varied from approximately 5.5% to 10.4%, depending on the sample type, with the highest and lowest uncertainty obtained for the PU4 and PU1 samples, respectively. An ANOVA test revealed that the probability (P) values for the WCA at varying T_c were 1.1E-12, which was significantly below 0.005, indicating a statistically significant difference in WCA among samples cured at different temperatures. This finding indicates that T_c plays a vital role in the WCA at $T_c \leq 140$ °C. Thus, the WCA value of the PU4 sample at the same T_c was higher than that of the PU2, which was attributed to an increase in the content of modified TiO_2 NPs with hydrophobic properties. Conversely, the effect of the weight content of TiO_2 NPs became more pronounced at $T_c > 160$ °C. Therefore, the T_c showed strong effects on the wettability behavior of the PU nanocomposite films: T_c less than 140 °C led to a stronger surface segregation of PU than T_c greater than 160 °C, resulting in increased WCAs.

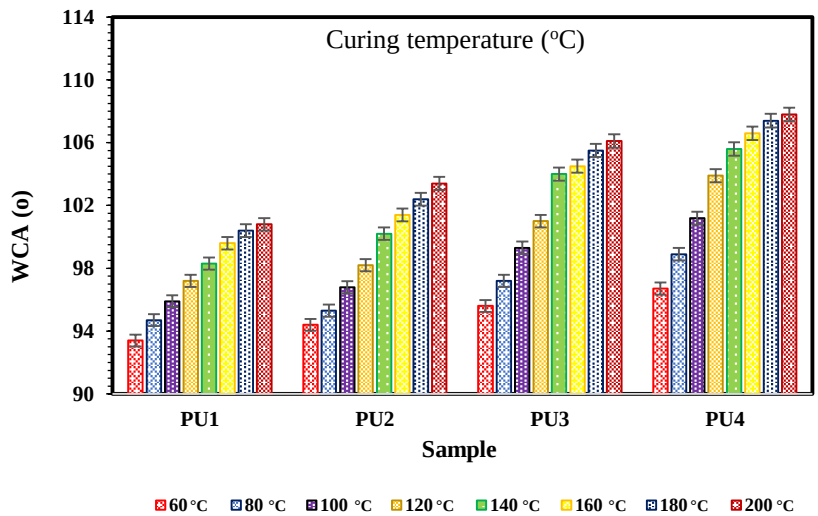

Figure 5: The results of WCA obtained from the PU1-4 samples cured at different T_c.

4.1.3. Moisture permeability study

The water absorption of the samples was determined experimentally by immersing them in water for a period of 30 days. Figure 6 shows the changes in the mass percentage of PU1-4 samples over extended exposure periods (in days). Error bars indicate the standard deviation corresponding to at least three experimental data points. The mass variations observed in all samples remain below 5 %, indicating a high level of moisture resistance. However, the presence of pore structures within the films was an important factor affecting the moisture permeability of samples. A consistent pattern is noted across all samples during the initial 20 days, wherein the rate of water absorption increases sharply with time, subsequently decelerating as exposure continues and ultimately stabilizing, resulting in an approximately constant weight.

After 20 days, the rate of water absorption in the samples decelerated, with a constant moisture content passing through the surface of the film over time. During the 25 days, the water absorption of the PU4 sample was lower than that of all other samples. This phenomenon is attributed to the hydrophobic characteristics of the PU4 sample, which initially prevented water penetration into the nanocomposite film.

After 25 days, the water absorption rate of the PU4 sample became slightly higher than the PU3, which is attributed to NPs agglomeration within the nano-composite film, leading to the formation of additional pores that allow for greater moisture penetration. In real conditions, water uptake correlates with an evolution of sample opacity. Two types of water molecules absorbed in a polymer matrix, including bound and free moisture, are reported in the literature [41]. The bound moisture is usually chemically bonded to the polymer matrix through the hydrolysis of the urethane group, resulting in chain scission in the polymer and leading to a significant modification of the tensile behavior of PU [38]. In contrast, the free moisture is located in the pores within the film, representing water penetration into the PU structure, which can be improved by an increase in the polyether diol content. Jin *et al.* [39] mentioned that one part of water molecules can penetrate the free volume of the polymer matrix, while others are bonded to hydrophilic groups such as hydroxyl (-OH), carbonyl groups to form hydrogen bonds with water molecules, leading to adsorption of water molecules in the PU network. Therefore, an increase in the water content within the film, via enhanced water exposure, leads to an increase in the chemical degradation products, including network chain cleavage at urethane groups that desorb slowly from the PU matrix during the exposure time.

Error analysis results showed that the uncertainty of the experimental data varied from approximately 7.1 to 11.4 %, depending on the sample type, with the highest and lowest uncertainty observed for the PU4 and PU1 samples, respectively. The ANOVA results showed that the *P*-values (probability>*F*) of mass change (%) in different samples was 2.35E-12, which was significantly less than 0.005, indicating a significant difference in the mass change of water molecules, as observed by the change in the weight content of TiO_2 NPs. The results indicated that the effect of the weight content of TiO_2 NPs on the mass change of samples was greater than the exposure time in the period of 20-30 days. In contrast, in the first 10 days, the effect of exposure time was greater than the weight content of TiO_2 NPs.

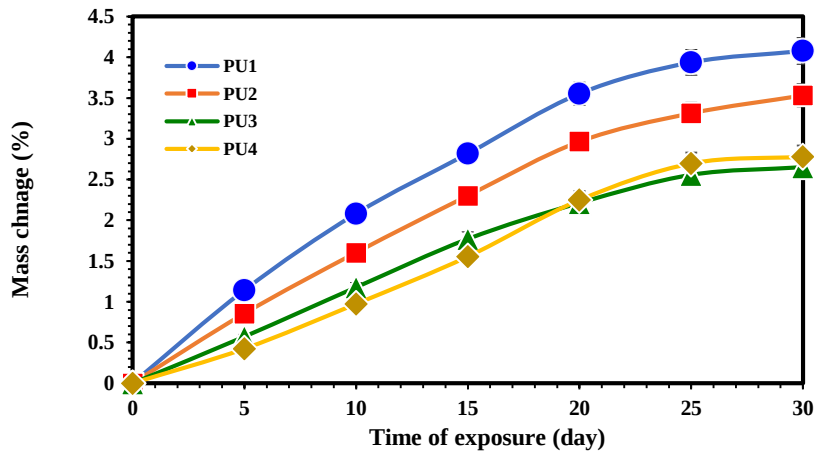

Figure 6: Variations of mass change (%) of PU1-4 samples with exposure time.

4.1.4. Thermal stability study

Figure 7 shows the appearance of the PU1-4 samples before (left images) and after (right images) curing at 180 °C with a constant rate of 10 °C/min in a nitrogen atmosphere. The selection of T_c is based on the degradation of the urethane linkage of PU into the form of isocyanate, alcohol, secondary amine, and carbon dioxide at 175 °C [40]. Lu [41] reported that the thermal degradation of PU occurs around or beyond the stability temperature of the urethane linkages. There are no visible defects such as the separation of TiO_2 NPs from the polymer matrix, non-uniform distribution of TiO_2 NPs, and dark color in the samples, which indicates a good mixing of TiO_2 NPs in the polymer matrix. The images of the samples before heating indicate that the incorporation of TiO_2 NPs into the PU matrix has no significant impact on the polymer matrix. The images clearly show the interconnected spherical micropores with size ranges of approximately 1-3 mm, which were created at the 3D structure within the nanocomposite film. The irregular porous structure of the film is the starting point for water penetration. Hydrophobic TiO_2 NPs are uniformly located in the soft phase to increase the thermal stability of the samples. However, the number of pores within the film slightly increases with an increase in the TiO_2 NPs wt.%. Kianpour *et al*. [6] reported that the phase separation in the nanocomposite film makes the amorphous segment more accessible, and as a result, degradation of amorphous regions leads to the formation of surface pores, which allow water molecules to penetrate the polymer and destroy it, forming interconnected pores in the PU@TiO_2 nanocomposite film.

The results indicate a high impact of TiO_2 NPs wt. % on the polymer structure and physical shape of samples when applying the heating process (right images). This effect is more clearly visible in the remaining films of PU1 and PU2 samples, which completely degrade under heating conditions. After heating, the micro-pores became inter-connected macro-pores at the 3D structures within the nanocomposite film. However, some cracks have been found in the PU2 and PU3 samples. The occurrence of solvent evaporation caused by the curing process led to chain entanglement and chemical processes, such as primary and secondary reactions of urethane, as well as the auto-oxidation of double bonds of alkyl chains, resulting in a cross-linked surface [27]. The results indicate that the incorporation of more than 3 wt. % TiO_2 NPs led to a significant decrease in the thermal degradation of the PU nanocomposite film.

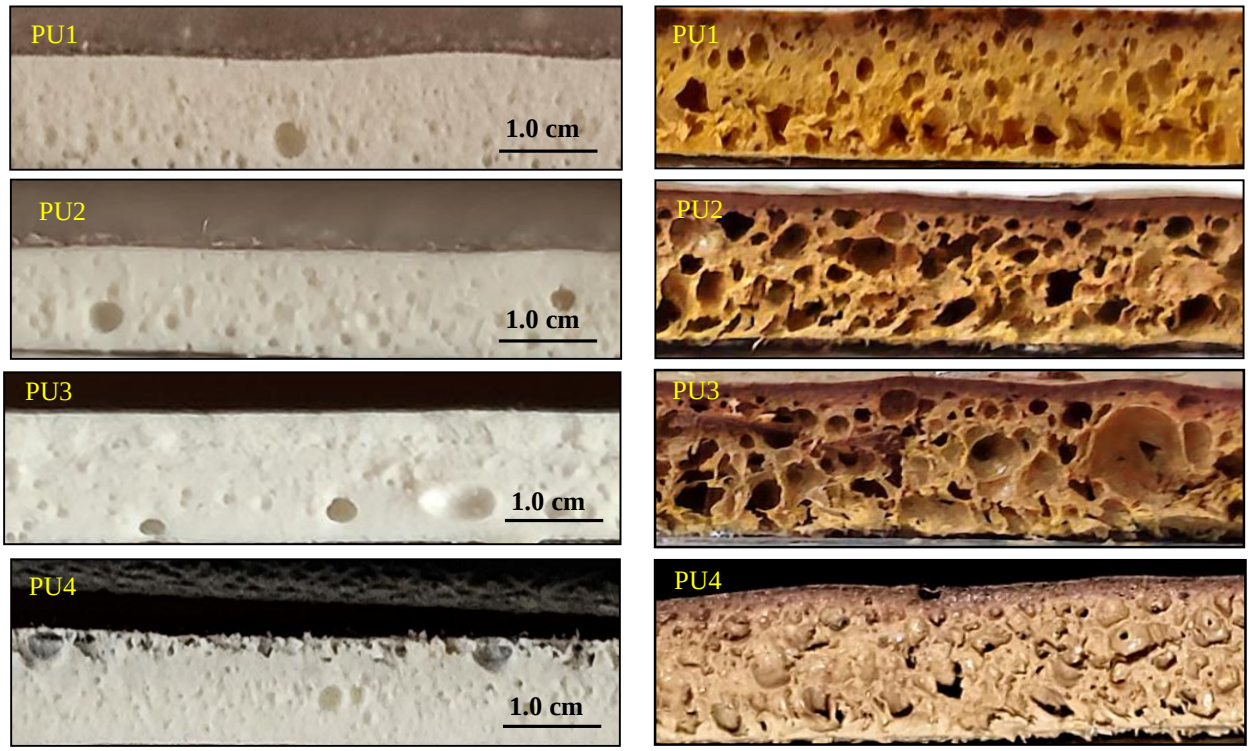

Figure 8: The effect of heating process on the PU1-4 samples (left and right images represent the samples before and after heating at 180 °C, respectively).

4.1.5. Thermogravimetric analysis

Figure 9 shows the (a) TGA and (b) DTG curves of PU1-4 samples at a constant heating rate of 2 °C/min under a nitrogen atmosphere. The weight loss profile of the samples exhibited a negligible weight loss of less than 0.3 wt. % within the temperature range of 25-135 °C. TGA curves of PU1-4 samples demonstrate three steps of degradation. The slope of the weight loss between 190-520 °C is not purely linear and can be divided into three degradation steps. The first degradation step, which occurs in the temperature range of 200-330 °C, results from the decomposition of the hard segment of urethane bonds, dependent on the NCO and -OH (alcoholic group) groups, as well as the evaporation of possible residual organic solvents in the polymer matrix [42]. The decomposed compounds include urethane, isocyanate and alcohol, primary or secondary amine and olefine, and CO_2 [37]. Zhou *et al.* [43] indicated that NCO consumption mainly occurs after two days of aging in water, which is highly dependent on the hydrolysis process that forms urea groups, while urethane formation with polyol is very limited in the reaction rate. They also reported that the NCO groups were consumed more rapidly by an increase in the exposure time, while continuous OH consumption resulted in a higher ratio of urethane/urea formation in the film.

The second degradation step is observed in the temperature range of 330-440 °C, which is attributed to the decomposition of soft segment chain scission of PU structure to release of volatile and residue compounds (Equation 4). The third degradation step occurs in the temperature range of 440-560 °C, which arises from the decomposition of unsaturated and saturated fatty acids through oxidation process of the residues to form of volatile and char compounds (equation 5). Branca *et al.* [44] showed that oxygen exerts a small influence on the primary and secondary decomposition steps of PU, while it affects significantly the breakage of the polymeric chains.

The results indicated that the thermal stability of the PU3 sample is slightly higher than that of PU4 due to the formation of pores within the nanocomposite film. The weight loss in the PU1 sample was determined to be about <0.5 , 46, and 22 % in the first, second, and third steps, respectively. In contrast, the weight loss of the PU4 sample was determined to be about <0.5 , 28, and 10 % in the first, second, and third steps, respectively. This result confirms that the weight loss of the PU4 sample is much lower than that of PU1, indicating the high thermal stability of the PU nanocomposite film. The possible reason for this behavior may be the decrease in the mobility of PU chains in the nanocomposite film, thereby showing the chain transfer reaction and thus slowing down the degradation process [35].

DTG curves of PU1-4 films show three endothermic peaks caused by three degradation steps, which are attributed to the interactions between the thermal degradation processes of hard and soft segments of the PU structure [2, 37]. The first distinct endothermic peak is located at about 270 °C, and is probably associated with the first step observed in the TGA curves, related to the hard segments. The second broad peak occurs at about 385 °C, which represents the results of the degradation of ester bonds in the soft segment. A small peak located above 455 °C represents the degradation of soft segments caused by a decrease in the NCO/OH molar ratio. Previous studies reported a direct relationship between

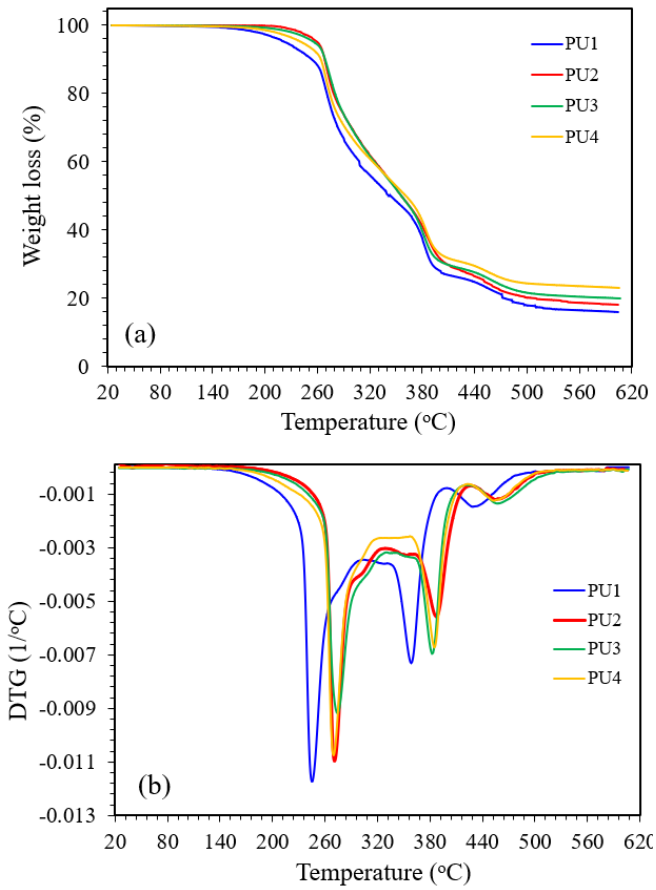

Figure 9: (a) TGA and (b) DTG curves of PU1-4 samples at a constant heating rate of 2 oC /min under nitrogen atmosphere.

the intensity of the DTG peaks and the NCO/OH molar ratio, where an increase in the peak intensity may be seen with an increase in the NCO/OH molar ratio [45, 46]. The obtained results confirm a relationship between DTG and TGA curves, where the onset of degradation is observed beyond these respective temperatures, and these endothermic peaks can be related to the phenomenon of melting points and molecular rearrangements.

Table 2 shows the results of the thermal analysis results of PU1-4 samples. The curing process was carried out at a constant heating rate of 2 ºC /min in a nitrogen atmosphere. The uncertainty of the mean experimental data is shown in the table, where high uncertainty of results was attributed to the PU4 samples. An increase in the weight content (%) of TiO_2 NPs led to a shift to higher T_g and also an increase in melting temperature T_m. Furthermore, an increase in the weight content (%) of TiO_2 NPs led to an increase in the char yield (%) of samples that cured at 600 ºC, which indicates the thermal stability of PU@TiO_2 nanocomposite films at high temperature. These results were in good agreement with the da Silva *et al*. [47] results that showed a slight increase in the T_g value indicates a reduction in the mobility of PU chains caused by the PU-TiO_2 interactions. A decrease in the molecular weight with the increase of the TiO_2 wt. % probably assigned to the variation in T_g values [47]. Krol et al. [16] reported stronger hydrogen bonding of soft segment microdomains by hard segments after the incorporation of TiO_2 into the PU matrix. In addition, an increase in the crystallinity can be seen by increasing the enthalpy of fusion (ΔH_m). da Silva *et al*. [47] reported an increase in the T_g value, proving a decrease in the mobility of polymer chains; thereby, T_g was shifted to higher temperatures due to TiO_2 incorporation. A similar effect was observed in the present study, and it was attributed to the hindrance in the macrochain mobility caused by TiO_2 NPs.

The melting energy will be higher as the weight content of TiO_2 NPs increases in the nanocomposite film. The presence of TiO_2 NPs requires a significant amount of enthalpy of fusion [48]. Therefore, an increase in ΔH corresponds to the additional weight content (%) of TiO_2 in the PU matrix; with a 7.0 wt.% addition of TiO_2 NPs, the enthalpy of fusion rise is about 22.82 J/g. The interaction between the surface-activated TiO_2 NPs and the PU solution is the primary reason behind the rise in ΔH, which leads to the formation of local agglomeration in the nanocomposite film [49].

4.1.6. Mechanical properties

Table 3 shows the results of the tensile test analysis of PU1-4 samples. The uncertainty of the experimental data is shown in the table. As indicated, the Young's modulus of the PU2 sample showed a slight increase compared with the PU1, which indicates that the presence of TiO_2 NPs led to difficulties in the mobility of polymer chains. An addition of 7 wt. % TiO_2 NPs led to a significant increase in the Young's modulus,

Table 2: Thermal analysis results of PU1-4 samples.

Sample	T_g (ºC)	T_m (ºC)	ΔH_m (J/g)	Char Yield (%) cured at 600 ºC
PU1	72.8±1.3	169.5±2.1	3.87±0.4	12.7±0.6
PU2	76.1±1.6	174.4±2.8	8.54±0.6	13.9±0.6
PU3	82.9±1.9	179.7±3.9	14.50±0.7	15.4±0.8
PU4	88.2±2.2	185.5±5.3	22.82±0.9	17.7±0.9

Table 3: Mechanical analysis results of PU1-4 samples.

Sample	Young's modulus (MPa)	Tensile strength (MPa)	Elongation at break (%)
PU1	16.67±0.8	42.1±2.5	522±4.6
PU2	18.78±0.9	40.3±3.7	515±4.8
PU3	23.87±1.0	39.4±4.1	509±5.1
PU4	31.36±1.3	38.6±4.4	501±5.4

by about two times. The tensile strength and tensile elongation at the break (%) gradually decrease, which indicates that adding TiO_2 NPs leads to a reduction in the interactions between the structure of the PU@TiO_2 nanocomposite film. The lowest value of elongation at break (%) for the PU4 sample compared with other samples indicate that the nanocomposite possesses increased crystallinity and strong interchain chemical bonding between the NPs and polymer matrix [47], as well as interfacial stress, or phase separation [48]. Pavlicevic´ *et al*. [15] reported that the addition of 2.0 wt. % titanium(IV) oxide NPs (TiO_2, Aeroxide) led to an increase in the hydrogen bonding index of the resulting nanocomposite from 72.4 wt. % of the pristine sample to 83.5 wt. %, which confirmed the uniform distribution of TiO_2 NPs in the PU matrix, avoiding NPs agglomeration in the nanocomposite film. It should be noted that the tensile strength of the PU4 sample still exhibits high elongation, making it suitable for use as a barrier coating without a significant decrease in the mechanical performance of the nanocomposite film.

Figure 10 shows the stress-strain analysis results of PU1-4 samples cured at 80 °C for 30 min. As expected, an increase in the TiO_2 wt. % led to change in the stress-strain curve of the sample, as the stress-strain curves changed from soft-flexible to the hard-flexible type. This result confirmed that the tensile strength of samples decreased with an increase in the TiO_2 wt. %, which attributed to improper damping ability of TiO_2 NPs [49, 50]. The nanocomposite film with 3 wt. % of TiO_2 (PU2 sample) showed slightly more stress to the deformation than pure PU film, while PU4 sample shows a maximum value of stress to a same deformation when compared to pure PU film. Therefore, PU4 become more fragile than the other samples due to an increase in the crosslink structures between the NPs and matrix of polymer or higher agglomeration of TiO_2 NPs, which cause high stress point in the polymer matrix, resulting in lower mechanical properties of sample, as reported by Zhang *et al*. [51]. Mergler and Schaake [52] reported that the stress-strain curves of nanocomposites tenacity could be attributed to the crystallinity degree of the films, and strength of bonding between adjacent polymer chains and their degree of orientation in the axis direction of nanocomposite. The stress-strain analysis showed that the coating with 3 wt. % of TiO_2 (PU2 sample) improved in its mechanical strength when compared to the other films.

Figure 11 shows the DMTA curves for the T_g of PU1-4 samples cured at 80 °C for 30 min. The peak position of tan δ gradually change from PU1 to PU4, where a change in the T_g of samples was observed by an increase in the TiO_2 wt.%. The pure PU had a T_g of ~72.8 °C, while its value was increased to 88.2 °C for PU4 sample. This result indicated that the PU4 sample had a lower damping capability than the pure PU (PU1 sample). A reduction in the damping capability cold be attributed to the interaction between polymer chain and NPs.

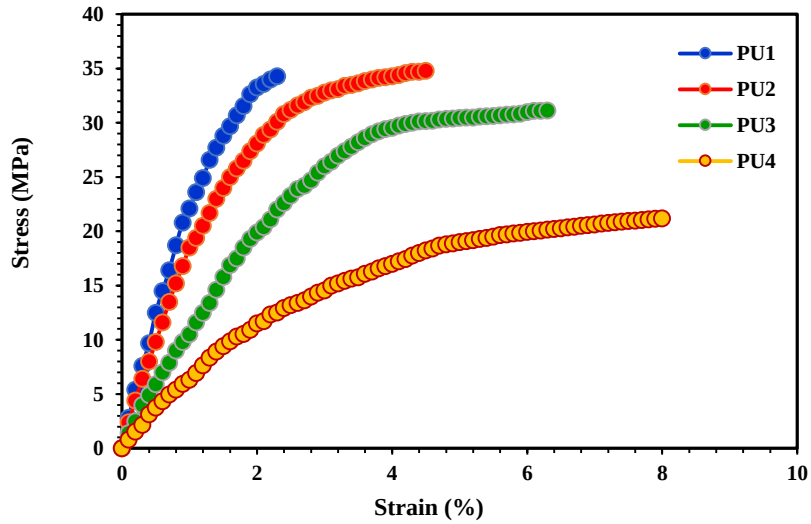

Figure 10: Stress-strain analysis results of PU1-4 samples cured at 80 °C for 30 min.

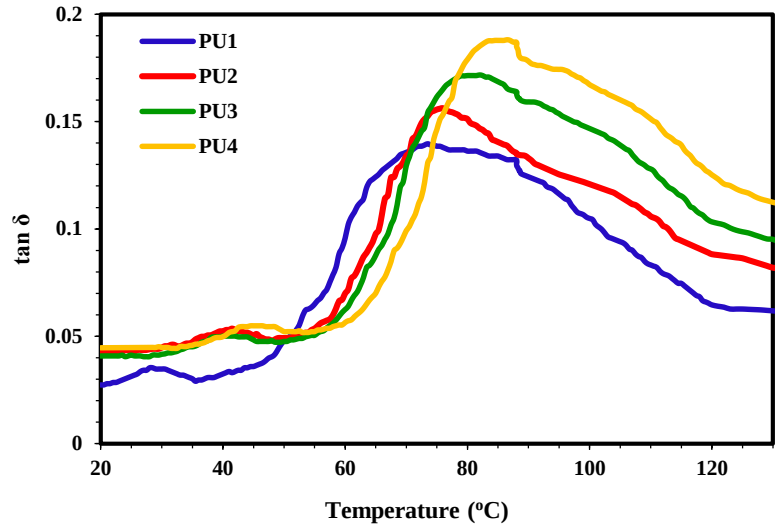

Figure 11: DMTA curves for the T_g of PU1-4 samples cured at 80 °C for 30 min.

Figure 12 shows the gel content (%) and solubility (%) results for the PU1-4 samples. The gel content (%) increases with an increase in the content of TiO_2 NPs wt.%, indicating a higher degree of crosslinking, and a reduction in the solubility (%) of the sample decreases with an increase in the TiO_2 wt. %. However, the low values of the gel content (5-20 %) represents a weakly crosslinked structure, in which the polymer matrix does not resist dissolution in the organic solvent during testing.

4.2. Theoretical modelling results

4.2.1. Kinetics of water sorption

Figure 13 shows the evolution of M_t/M_∞ as a function of the square root of time ($t^{1/2}$) for different PU1-4 samples. The points represent the experimental data obtained from Figure 6, while the lines represent the estimated results obtained from the Fick's diffusion law. The input data of M_t/M_∞ are obtained experimentally for the PU1-4 samples at the same T_c of 80 °C. As can be seen, the sorption curves represent a sigmoid shape caused by two distinct trends found in the curves. This type of sorption isotherm is called a type III isotherm in reference to the BET classification. Slow transport of water molecules within the PU film is controlled by simultaneous kinetic models of adsorption and diffusion of water sorption.

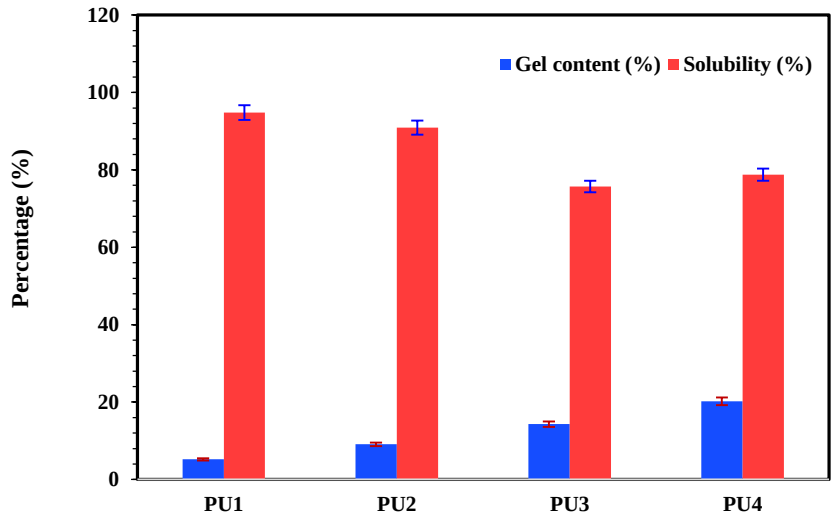

Figure 12: Gel content (%) and solubility (%) results for the PU1-4 samples.

In the first 2 days, the results indicate that M_t/M_∞ follows a linear trend with $t^{1/2}$ in the early stages and then abruptly increases with an increase of $t^{1/2}$. After 10 days ($t^{1/2}$ more than 1500 $s^{0.5}$), M_t/M_∞ reaches a constant value, known as sorption equilibrium, which represents a linear shape of water sorption curves as a function of the square root of time. This result indicates that the water sorption mechanism within the film obeys the Fick model. In addition, M_t/M_∞ increases with an increase in the weight content of TiO_2 NPs, which indicates fast kinetics of water sorption. The *D* values were calculated based on the different PU1-4 samples to evaluate the effect of the content of TiO_2 NPs on the kinetics mechanism of water sorption within the PU film.

By comparing the results, both experimental data (Figure 6) and theoretical results (Figure 13) confirmed that water sorption within the PU@TiO_2 films includes two stages: diffusion of concentration gradient and absorption of water into the PU network, which necessitates consideration of the interaction between water molecules and the PU network. In the early stage of water absorption, the free water molecules do not interact with the PU network; therefore, their movement rate is fast, while the bound water interacting with the PU network moves slowly [35]. Therefore, Fick's diffusion law can simply describe the early stage of water absorption behavior onto the PU network. The second stage of water absorption occurs over time, where water molecules can enter the interior of the PU network and interact with the polymer. Thus, Fick's law is no longer applicable because it does not take into account the interaction between water molecules and the PU network.

Figure 14 shows the variation of D_{eff} of water vapor related to *RH* in different PU1-4 samples. Points represent the experimental data, while the dashed lines indicate the exponential fit of data obtained from the theoretical results. The water vapor sorption was approximately linear at a mass fraction in the range of 0.0-0.5, which follows Fick's law. D_{eff} was calculated from the slope of the linear section. The slope of the curve decreased when *RH* reached saturation state. As expected, D_{eff} increased with an increase in *RH* due to higher absorption of water molecules in the samples. In addition, D_{eff} decreased with an increase in the weight content of TiO_2 NPs. At 50 % *RH*, D_{eff} f or the PU1 sample was calculated to be 2.4×10^{-8} $cm^2.s^{-1}$, while a decrease in the D_{eff} value of around (1.4-2.3) $\times10^{-10}$ $cm^2.s^{-1}$ was obtained for the PU2-4 samples. This result indicates that the value of D_{eff} is dependent on the TiO_2 NPs wt. %. Water molecules penetrate more readily through the internal micropores of the nanocomposite film, which provide high free volume for water, ultimately contributing to comparable overall water absorption rates.

At 50 % *RH*, a minimum value of 1.4×10^{-10} $cm^2.s^{-1}$ is obtained for the PU3 sample with the lowest porosity within the film. This result indicates that D_{eff} is highly affected by the structure of the nanocomposite film. At 70 % *RH*, the mass fraction of water vapor sorption increased immediately with a non-linear trend to reach the equilibrium state at an *RH* of 90 %, which can be explained by saturation [27].

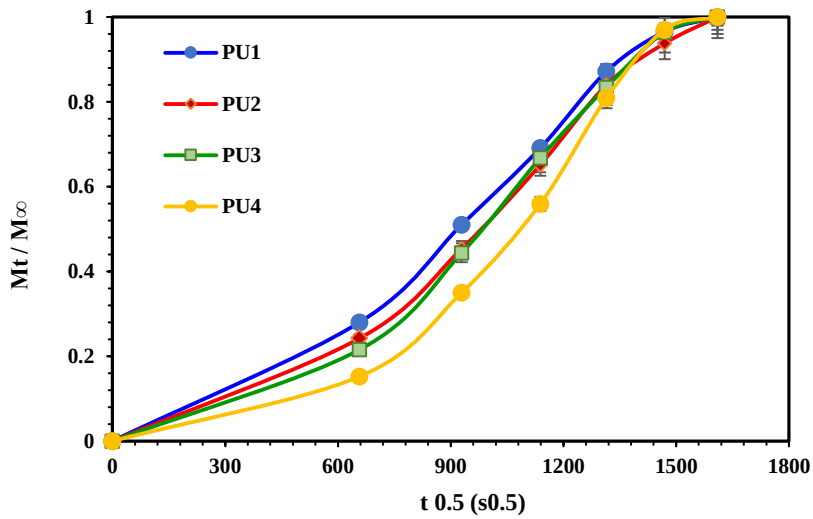

Figure 13: Evolution of M_t/M_∞ as a function of $t^{1/2}$ for different PU1-4 samples.

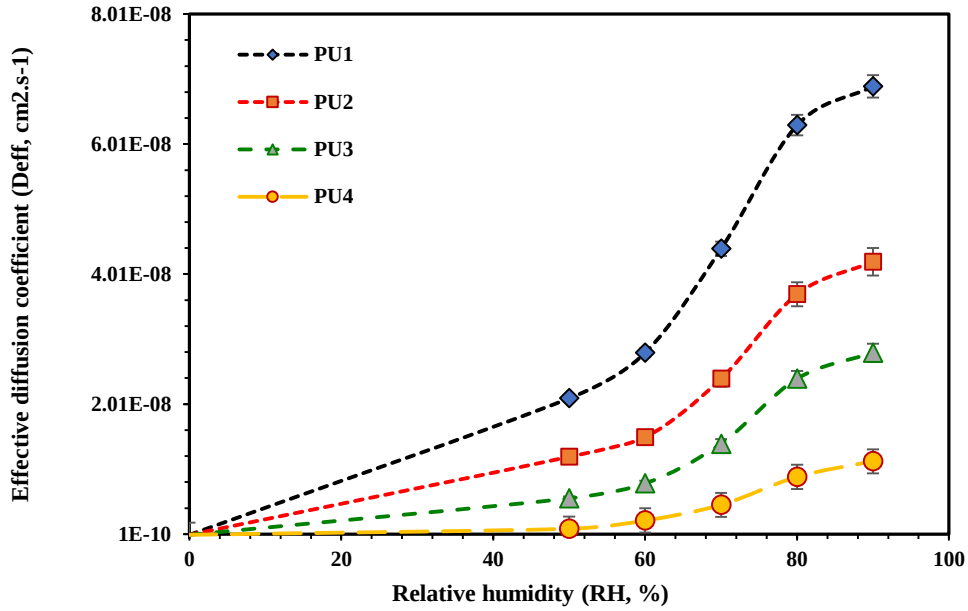

Figure 14: Variation of D_{eff} of water vapor molecules related to relative humidity (*RH*) for different PU1-4 samples.

Based on the ANOVA results, the effect of *RH* on the D_{eff} was higher than the weight content of TiO_2 NPs. An increase in the *RH* from 50 to 90 % led to a 63 % increase in the $D_{eff.}$ In contrast, an increase in the weight content of TiO_2 NPs from 3 to 7 % led to a 13 % increase in $D_{eff.}$ The discrepancy in the calculated D_{eff} values is caused by two reasons: (1) a difference in the sorption mechanism and transport of water vapor molecules within the PU nanocomposite film. The water-water and water-soft/hard segment interactions become experimentally predominant phenomena, leading to a decrease in the D_{eff} of samples. (2) The effect of non-homogeneities in the film structure, which is caused by a reduction in the density of the PU samples and an increase in the chain mobility of the film. Therefore, the incorporation of TiO_2 NPs into the PU matrix led to a change in the water sorption kinetics and physical properties of the PU film.

Figure 15 shows the variation of the P_{eff} of water vapor related to *RH* for different PU1-4 samples. P_{eff} follows a linear trend with RH in the early stage and then exponentially increases with an increase in the *RH*. Additionally, P_{eff} significantly increased with an increase in the weight content of TiO_2 NPs. Points represent the experimental data, while the dashed lines indicate the exponential fit of data obtained from the theoretical results. At 50 % *RH*, P_{eff} for the PU1 sample was calculated to be 3.6×10^{-9} mg.cm $(Pa.s)^{-1}$, while a decrease in the P_{eff} value around $(3.2\text{-}8.0)\times10^{-11}$ mg.cm $(Pa.s)^{-1}$ is obtained for the PU2-4 samples. This result shows that the value of P_{eff} is highly dependent on the TiO_2 NPs wt. %. At 50 % *RH*, a maximum value of 8.0×10^{-11} mg.cm $(Pa.s)^{-1}$ is obtained for the PU4 sample with a porous structure compared to the other nanocomposite films (PU2-3). This result indicates that P_{eff} is significantly affected by the pores and channels within the nanocomposite film. This result is confirmed by the fact that the pore structure is an important factor affecting the water permeation mechanism. On the other hand, surface roughness has a significant effect on the moisture permeate flux. In the case of the PU1 sample with a smooth surface, a higher permeate flux, resulting in higher P_{eff} values, was ultimately obtained compared to the PU4 sample with a rough surface. This result was in good agreement with the literature [53], which indicates that more hydrophobic and rougher surfaces typically show decreased permeate fluxes due to facile attachment and agglomeration of NPs on the film surface.

At 70 % *RH*, P_{eff} increases significantly with an increase in the *RH*, where an equilibrium state was achieved at an *RH* of 90 %. These results indicate that the porous structure of the nanocomposite film has a dominant role in permeability at higher *RHs*. Based on the ANOVA results, the effect of the weight content of TiO_2 NPs on the P_{eff} was greater than that of the *RH*. An increase in the weight content of TiO_2 NPs from 3.0 to 7.0 wt. % led to a 31 % increase in the P_{eff}, while an increase in the *RH* from 50 to 90 % led to an increase of 18 % in the $P_{eff.}$

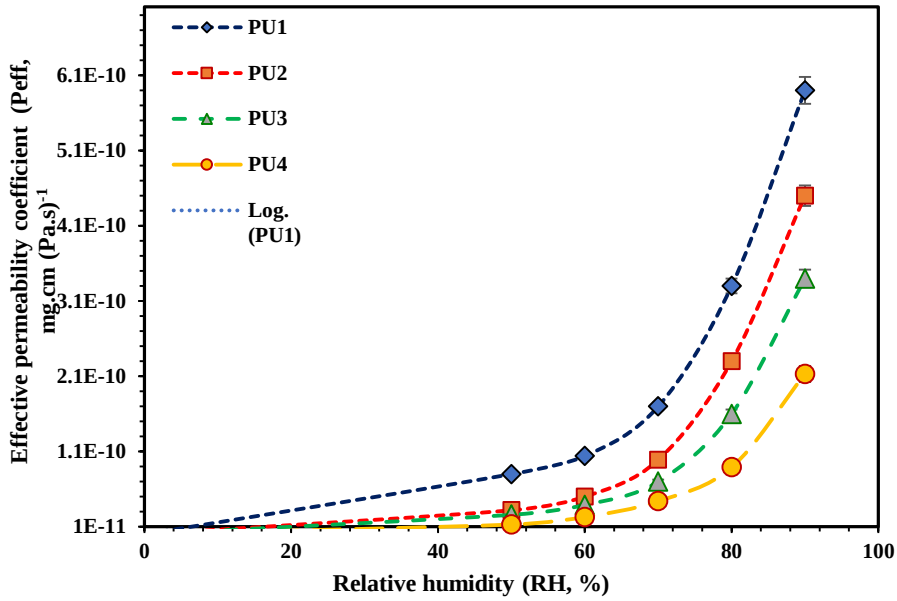

Figure 15: The variation of effective permeability coefficients (P_{eff}) of water vapor molecules related to *RH* for different PU1-4 samples.

4. Conclusions

In summary, the surface wettability, moisture permeability, mechanical durability, and thermal stability of pure polyurethane (PU) and PU-based nanocomposite films incorporated with TiO_2 nanoparticles (NPs) (3, 5, and 7 wt. %) were studied experimentally. The effective diffusion coefficient (D_{eff}) and permeability coefficient (P_{eff}) of water vapor sorption were determined theoretically based on the kinetic model of water absorption. Our results are as follows:

1. In contrast to the pure PU film, which has a smooth surface with low average surface roughness, the PU@TiO_2 nanocomposite film is homogeneously covered by TiO_2 NPs. However, an increase in the NP weight content led to an increase in the surface roughness of the films from 69.224 to 142.429 nm, caused by local NP agglomeration.
2. The water contact angle of the films increased from 94.7° to 98.9° with the increase in the film's surface roughness, which is also caused by local NP agglomeration. Furthermore, an increase in the NP weight content led to an enhancement of the hydrophobic properties of the film.
3. The curing temperature (T_c) showed an important effect on the wettability behavior of the films. At $T_c \leq 140$ °C, a high surface segregation of the nanocomposite film was observed compared to $T_c >$ 160 °C. An increase in T_c led to an increase in the hydrophobicity of the PU nanocomposite film, which is attributed to a decrease in the surface interactions of fluid-solid on the film surface, resulting in a low value of the water contact angle. The WCA value of pure PU increased from 93.4° to 107.1° with an increase in T_c from 60 to 200 °C, respectively.
4. The moisture permeability of a pure PU sample improved by incorporating 5 wt.% TiO_2 NPs. In contrast, the water absorption rate of the 7 wt.% sample became slightly higher than the 5 wt.% sample. Agglomeration phenomena led to the formation of additional pores and porous structures in the bulk of the film, facilitating moisture penetration within the film.
5. The thermal stability and mechanical durability of the samples increases with an increase in the weight content of TiO_2 NPs. The glass transition temperature (T_g), melting temperature (T_m) and char yield (%) of the samples increased with NP content. T_m and T_g values of sample (7 wt.%) were 88.2 and 185.5 °C, respectively, while the enthalpy of fusion was determined to be 22.82 J/g. An increase in the NP weight content led to a shift to a higher glass transition temperature from 72.8 to 88.2 °C and also an increase in the melting temperature of the nanocomposite film from 169.5 to 185.5 °C. In contrast,

an incorporation of more than 3 wt. % NPs led to a significant decrease in the thermal degradation of the film. The results indicated that the structure change at 270 °C is mainly due to the three-step degradation of the urethane linkage.

6. The theoretical results indicate that D_{eff} is highly affected by the porous structure of the sample. D_{eff} decreased from 1.4×10^{-10} to 2.4×10^{-8} $cm^2.s^{-1}$ because of an increase in the NP weight content from 3 to 7 wt. %, while the permeability coefficient (P_{eff}) exhibited a significant increase from 3.2×10^{-11} to 8.0×10^{-11} mg.cm(Pa.s)$^{-1}$. The values of D_{eff} and P_{eff} increased with an increase in the relative humidity (*RH*) due to the high absorption of water molecules in the samples. The effect of *RH* on D_{eff} is greater than the NP weight content, while the inverse behavior is concluded for P_{eff}.

Acknowledgments

The author would like to thank Hamedan University of Technology (Grant No. 403/6640).

5. References

1. Bayer O. Das di-isocyanat-Polyadditionsverfahren (Polyurethane). Angew Chem. 1947;59(1):257-272. https://doi.org/10.1002/ange.19470590901
2. Xiao Ch, Bai Y, Pu Y, Luo H, Xiao S, He B. Effect of polymer architecture and hard/soft segment ratio on the surface morphology and mechanical properties of polyurethane films for potential orthodontic treatment. J Appl Polym Sci. 2020; 137(1):e49363. https://doi.org/10.1002/app.49363
3. Ma Y, Wu LF, Li SL, Han X, Peng XY, Feng YM, Ji YM, Yang YK, Liu F. Regulating the structure of thermoplastic polyurethane elastomers with a diol chain extender to strength Performance. J Appl Polym Sci. 2023;140(22):e53921. https://doi.org/10.1002/app. 53921
4. Shi Zh, Sheng Y, Wu J, Cui J, Lin W, Ngai T. Porous waterborne polyurethane films templated from pickering foams for fabrication of synthetic leather. Langmuir. 2024;40(1):475-4761. https://doi.org/10.1021/acs.langmuir.3c03514
5. Kasanen J, Suvanto M, Pakkanen TT. UV stability of polyurethane binding agent on multilayer photo-catalytic TiO_2 coating. Polym Test. 2011; 30 (2): 381-389. https://doi.org/10.1016/j.polymertesting.2011.02.006
6. Kianpour Gh, Bagheri R, Pourjavadi A, Ghanbari H. In situ synthesized TiO_2-polyurethane nanocomposite for bypass graft application: In vitro endothelialization and degradation. Mat Sci Eng C. 2020; 114(1): 111043. https://doi.org/10.1016/j.msec.2020.111043
7. Jakhmola S, Das S, Dutta K. Emerging research trends in the field of polyurethane and its nanocomposites: Chemistry, synthesis, characterization, application in coatings and future perspectives. J Coat Technol Res. 2024; 21(1):137-172. https://doi.org/10.1007/s11998-023-00841-z
8. Samimi A. Use of polyurethane coating to prevent corrosion in oil and gas pipelines transfer. IJIAS 2012; 1(2):186-193. http://www.issr-journals.org/ijias.
9. Sabah Khadim N, AbdulKareem Abdulaali N, Saleh HM. Study of Heavy metal ions adsorption using grafted polyurethane with iron oxide nanoparticles as adsorbent. J Nanostruct. 2023;13(1):173-183. https://doi.org/10.22052/JNS.2023.01.019.
10. Hanoon RS, Al-Lami AKA, Abbas AM. Polyurethane/Silver nanoparticle composite thermal behavior and electrical conductivity enhancement. J Nanostruct. 2024;14(1):38-47. https://doi.org/10.22052/JNS.2024.01.004
11. Pei A, Malho J-M, Ruokolainen J, Zhou Q, Berglund LA. Strong nanocomposite reinforcement effects in polyurethane elastomer with low volume fraction of cellulose nanocrystals. Macromol. 2011; 44(11):4422-4427. https://doi.org/10.1021/ma200318k.
12. Madbouly SA, Xia Y, Kessler MR. Sustainable polyurethane-lignin aqueous dispersions and thin films: Rheological behavior and thermomechanical properties. ACS Appl Polym Mater. 2020; 2(11): 5198-5207. https://doi.org/10.1021/acsapm.0c00954.
13. Zhang Y, Liu Z, Han Y, et al. Preparation and performance of waterborne polyurethane composite coatings for electromagnetic interference shielding. J Coat Technol Res. 2025;22(3):1079-1086. https://doi.org/10.1007/s11998-024-01033-z
14. Chen D, Liu Y, Zhang Z, Li Sh, Yang K, Li Zh. Ingeniously incorporating hollow mesoporous silica into waterborne polyurethane film to improve water vapor permeability. Mat Lett. 2022; 326(1):132994. https://doi.org/10.1016/j.matlet.2022.132994
15. Pavlicevic J, Spirkova M, Aroguz A, Jovicic M, Kojic D, Govedarica D, Ikonic B. The effect of TiO_2 particles on thermal properties of polycarbonate-based polyurethane nanocomposite films. J Thermal Anal Calor.2019;60(1):1-14. https://doi.org/10.1007/s10973-019-08750-3
16. Krol P, Szlachta M, Pielichowska K. Hydrophilic and hydrophobic films based on polyurethane cationomers containing TiO_2 nanofiller. Prog Org Coat. 2022;162 (1):106524. https://doi.org/10.1016/j.porgcoat.2021.106524.

17. Bahramian A. Poly (ethylene terephthalate)-based nanocomposite films as greenhouse covering material: Environmental sustainability, mechanical durability, and thermal stability. J Appl Polym Sci. 2020; 138(1):e49991. https://doi.org/10.1002/app.49991
18. Pegoretti A, Fambri L, Penati A, Kolarik J. Hydrolytic resistance of model poly(ether urethane ureas) and poly(esterurethane ureas). J Appl Polym Sci. 1998;70(3):577-586. https://doi.org/10.1002/(SICI)1097-4628(19981017)70:3<577::AID-APP20>3.0.CO;2-X.
19. Burgaz E, Kendirlioglu C. Thermomechanical behavior and thermal stability of polyurethane rigid nanocomposite foams containing binary nanoparticle mixtures. Polym Test. 2019;77(1):105930. https://doi .org/10.1016/j.polymertesting.2019.105930.
20. Lin Ch-Y, Liao K-H, Su Ch-F, Kuo Ch-H, Hsieh K-H. Smart temperature-controlled water vapor permeable polyurethane film. J Memb Sci. 2007; 299 (1-2):91-96. https://doi.org/10.1016/j.memsci.2007.04.028.
21. Li K, Peng J, Zhang M, Heng J, Li D, Mu Ch. Comparative study of the effects of anatase and rutile titanium dioxide nanoparticles on the structure and properties of waterborne polyurethane. Colloid Surf A: Physicochem Eng Asp. 2015; 470(1):92-99. https://doi.org/10.1016/j.colsurfa.2015.01.072.
22. Rudlong AM, Goddard JM. Synthesis and characterization of hydrophobic and low surface tension polyurethane. Coating. 2023; 13(7):1133. https://doi.org/10.3390/coatings13071133.
23. Xue M, Ji Y, Ou J, Wang F, Li Ch, Lei Sh, Li W. Surface wettability and strong adhesion of medical polyurethane elastomer porous films by microphase separation. AIP Adv. 2019;9(1):075309. https://doi.org/10.1063/1.5111008.
24. Mirzadeh S, Asefnejad Az, Khonakda HA, Jafari SH. Improved surface properties in spray-coated PU/TiO_2/graphene hybrid nanocomposites through nonsolvent-induced phase separation. Surf Coat Technol. 2021;405(1):126507. https://doi.org/10.1016/j.surfcoat.2020.126507.
25. Bhaliya JD, Raju Kutcherlapati SN, Dhore N, Punugupati N, Lekha Sunkara K, Misra S, and Kumar Joshi ShSh, Soybean oil-derived, non-isocyanate polyurethane-TiO_2 nanocomposites with enhanced thermal, mechanical, hydrophobic and antimicrobial properties, RSC Sustain. 2025; 3(1):1434-1447. https://doi.org/10.1039/d4su00587b.
26. Possart W, Zimmer B. Water in Polyurethane Networks: Physical and chemical ageing effects and mechanical parameters. Contin Mech Thermodyn. 2024; 36(1):261-287. https://doi.org/10.1007/s00161-022-01082-y.
27. Turan D. Water Vapor Transport properties of polyurethane films for packaging of respiring foods. Food Eng Rev. 2019;13(1):54-65. https://doi.org/10.1007/s12393-019-09205-z
28. Dolmaire N, Espuche E, Mechin F, Pascault J-P. Water transport properties of thermoplastic polyurethane films. J Polym Sci Part B Polym Phys. 2004; 42(3):473-492. https://doi.org/10.1002/polb.10708.
29. Barrie JA, Numm A, Sheer A. The sorption and diffusion of water in polyurethane elastoners. In: Hopfenberg HB, ed. Permeability of Plastic Films and Coatings. pp. 167-168. 1974.
30. Zisman WA. Relation of the equilibrium contact angle to liquid and solid constitution. Adv Chem. 1964; 9(43):1-51. https://doi.org/10.1021/ba-1964-0043.ch001.
31. Schmid M, Dallmann K, Bugnicourt E, Cordoni D, Wild F, Lazzeri A, Noller K. Properties of whey-protein-coated films and laminates as novel recyclable food packaging materials with excellent barrier properties. Int J Polym Sci. 2012;1(1):1-7. https://doi .org/10.1155/2012/562381
32. Crank J. The mathematics of diffusion. 2nd Ed. Clarendon Press, Oxford; 1979.
33. Deb S, Braden M, Bonfield W. Water absorption characteristics of modified hydroxyapatite bone cements. Biomater. 1995;16(14):1095-1100. https://doi. org/10.1016/0142-9612(95)98906-U
34. Zare Y, Study of Nanoparticles aggregation/ agglomeration in polymer particulate nanocomposites by mechanical properties, Composites Part A Appl Sci Manuf. 2016; 84(1):158-164. https://doi.org/10.1016/j.compositesa.2016.01.020.
35. Wang C, Xu Z, Xia Y, Zhang Ch, Fang H, Sun K. Water transport mechanism and performance evaluation in polyurethane materials: A state-of-the-art review. Polym Test. 2024; 138(1):108554. https://doi.org/10.1016/j.polymertesting.2024.108554.
36. Wang Y, Hansen ChJ, Wu Ch-Ch, Robinette EJ, Peterson AM. Effect of surface wettability on the interfacial adhesion of a thermosetting elastomer on glass. RSC Adv. 2021; 11(49):31142-31151. https://doi.org/10.1039/D1RA05930D.
37. Alam M, Alandis NM, Zafar F, Sharmin E, Al-Mohammadi YM. Polyurethane-TiO_2 nanocomposite coatings from sunflower-oil-based amide diol as soft segment. J. Macromol Sci Part A Chem. 2018;55 (10): 698-708. https://doi.org/10.1080/10601325.2018.1496945.
38. Le Gac PY, Choqueuse D, Melot D. Description and modeling of polyurethane hydrolysis used as thermal insulation in oil offshore conditions. Polym Test. 2013;32(8):1588-1593. https://doi.org/10.1016/j. polymertesting.2013.09.005.
39. Jin X, van der Sman RGM, van Maanen JFC. Moisture sorption isotherms of broccoli interpreted with the Flory-Huggins free volume theory. Food Biophys. 2014;9(1):1-9. https://doi.org/10.1007/s11483- 013-9320-7.
40. Sui H, Ju X, Liu X, Cheng K, Luo Y, Zhong F. Primary thermal degradation effects on the polyurethane film. Polym Degrad Stab. 2014;101 (1):109-113. https://doi.org/10.1016/j.polymdegradstab. 2013.

12.023.
41. Lu Q-W, Macosko ChW, Horrion J. Compatibilized blends of thermoplastic polyurethane (TPU) and polypropylene. Macromol Symp. 2003; 198(1):221-232. https://doi.org/10.1002/masy.200351102.
42. Coutinho FMB, Delpech MC. Degradation profile of films cast from aqueous polyurethane dispersions. Polym Degrad Stab. 2000; 70(1):49-57. https://doi.org/10.1016/S0141-3910(00)00124-0
43. Zhou H, Liu Y, Lu Y, Tran K. Monitoring the reaction kinetics of waterborne 2-pack polyurethane coatings in the dispersion and during film formation. CJCE 2022;100(4):703-713. https://doi.org/10.1002/cjce.24287
44. Branca C, Di Blasi C, Casu A, Morone V. and Costa C, Reaction kinetics and morphological changes of a rigid polyurethane foam during combustion, Thermochim Acta. 2003;399(1-2):127-137. https://doi. org/10.1016/S0040-6031(02)00455-0.
45. Somani KP, Patel NK, Kansara SS, Rakshit AK. Effect of chain length of polyethylene glycol and crosslink density (NCO/OH) on properties of castor oil based polyurethane elastomers. Polym Sci Part A: Polym Chem. 2006;43(4-5):797-811. https://doi.org/10.1002/pola.20944 .
46. Morel A, Salaun F, Bedek G, Dupont D, Giraud S. Water vapor permeability of thermosensitive polyurethane films obtained from isophorone diisocyanate and polyester or polyether polyol. J Mater Sci. 2017; 52(1):1014-1027. https://doi.org/10.1007/s10853-016-0483-8.
47. da Silva VD, dos Santos LM, Subda SM, Ligabue R, Seferin M, Carone CLP, Einloft S. Synthesis and characterization of polyurethane/titanium dioxide nanocomposites obtained by in situ polymerization. Polym Bull. 2013;70(1):1819-1833. https://doi.org/10.1007/s00289-013-0916-6.
48. kheyrandish M, Bafande F, Sheikh Arabi M, Features and methods of making nanofibers by electrospinning, phase separation and self-assembly, Jorjani Biomedicine J. 2022;10(1):13-25, https://doi.org/10.29252/ jorjanibiomedj.10.1.13.
49. Liu Y, Yang L, Ma C, Zhang Y. Thermal behavior of sweet potato starch by non-isothermal thermos-gravimetric analysis. Materials. 2019;12(5):699. https://doi.org/10.3390/ma12050699.
50. Hakke VS,Landge VK, Sonawane ShH, Uday G, Babu Bh, Ashokkumar M, Erico MM. The physical, mechanical, thermal and barrier properties of starch nanoparticle (SNP)/Polyurethane (PU) nanocomposite films synthesized by an ultrasound-assisted process. Ultrason Sonochem. 2022; 88 (1):106069. https://doi.org/10.1016/j.ultsonch.2021.106069.
51. Zhang SW, Liu R, Jiang JQ, Yang C, Chen M, Liu XY. Facile Synthesis of Waterborne UV-Curable Polyurethane/Silica Nanocomposites and Morphology, Physical Properties of Its Nanostructured Films. Prog Org Coat. 2011;70(1):1-8. https://doi.org/10.1016/j.porgcoat.2010.09.005
52. Mergler Y, Schaake R. Relation between strain hardening and wear resistance of polymers, J Appl Polym Sci. 2004;92(1):2689. https://doi.org/10.1002/app.20251.
53. Woo SH, Park J, Min BR. Relationship between permeate flux and surface roughness of membranes with similar water contact angle values, Sep Purif Technol. 2015;146(1):187-191. http://dx.doi.org/10.1016/j.seppur.2015.03.048.

How to cite this article:
Karimi N, Bahramian A. Polyurethane-based Nanocomposite Film as Barrier Coating: Effect of Weight Content of TiO_2 Nanoparticles on the Surface Wettability, Moisture Permeability, Mechanical Durability, and Thermal Stability. Prog Color Colorants Coat. 2026;19(4):485-506. https://doi.org/10.30509/pccc.2025.167696.1460